# Enhancing the Hole-Conductivity of Spiro-OMeTAD without Oxygen or Lithium Salts by Using Spiro(TFSI)$_2$ in Perovskite and Dye-Sensitized Solar Cells

William H. Nguyen,[§] Colin D. Bailie,[†] Eva L. Unger,[†] and Michael D. McGehee*,[†]

[§]Department of Chemistry and [†]Department of Materials Science and Engineering, Stanford University, Stanford, California 94305, United States

Ⓢ *Supporting Information*

ABSTRACT: 2,2′,7,7′-Tetrakis(*N,N*-di-*p*-methoxyphenyl-amine)-9,9′-spirobifluorene (spiro-OMeTAD), the prevalent organic hole transport material used in solid-state dye-sensitized solar cells and perovskite-absorber solar cells, relies on an uncontrolled oxidative process to reach appreciable conductivity. This work presents the use of a dicationic salt of spiro-OMeTAD, named spiro(TFSI)$_2$, as a facile means of controllably increasing the conductivity of spiro-OMeTAD up to 10^{-3} S cm^{-1} without relying on oxidation in air. Spiro(TFSI)$_2$ enables the first demonstration of solid-state dye-sensitized solar cells fabricated and operated with the complete exclusion of oxygen after deposition of the sensitizer with higher and more reproducible device performance. Perovskite-absorber solar cells fabricated with spiro(TFSI)$_2$ show improved operating stability in an inert atmosphere. Gaining control of the conductivity of the HTM in both dye-sensitized and perovskite-absorber solar cells in an inert atmosphere using spiro(TFSI)$_2$ is an important step toward the commercialization of these technologies.
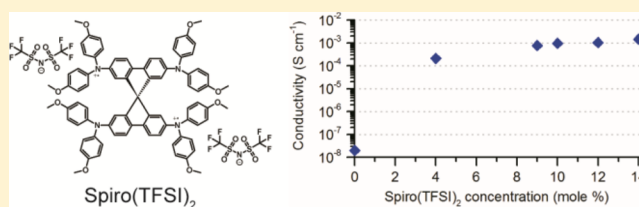
INTRODUCTION

Solid-state dye-sensitized solar cells (ssDSSCs) and, more recently, perovskite-absorber solar cells (PSCs) have experienced a remarkable increase in solar cell device efficiencies.[1−4] Though PSCs have reached certified efficiencies over 17%, they suffer from large variations in device performance and reproducibility.[1,3,5,6]

2,2′,7,7′-Tetrakis(*N,N*-di-*p*-methoxyphenylamine)-9,9′-spirobifluorene, abbreviated as spiro-OMeTAD, is the prevalently used hole transporting material (HTM) in ssDSSCs and PSCs. The lack of reproducibility in these devices stems partly from the low intrinsic hole-mobility and -conductivity of spiro-OMeTAD as well as the necessity to dope the HTM p-type to improve its conductivity.[7,8] Chemical dopants such as N(PhBr)$_3$SbCl$_6$ were first introduced to oxidize, and thus p-dope spiro-OMeTAD, but were rapidly replaced by the more effective additive lithium bis(trifluoromethanesulfonyl)imide (LiTFSI).[7,9,10] Unlike chemical oxidants, LiTFSI does not directly oxidize spiro-OMeTAD and instead promotes the oxidative reaction between spiro-OMeTAD and oxygen in the presence of either light or thermal excitation.[11,12]

Because doping spiro-OMeTAD with LiTFSI necessitates an open system to allow the ingress of oxygen, it is difficult to control the amount of oxidized spiro-OMeTAD formed and obtain consistent results. The concentration of oxidized spiro-OMeTAD in the HTM has been shown to be dependent on a number of factors including light intensity and the concentrations of Li$^+$ ions and oxygen present in the film.[10,12,13] The formation of oxidized spiro-OMeTAD has also been shown to be reversible during device operation in air depending on the

preconditioning of the device and sweep direction of the current−voltage measurement.[11−13] Unpredictable variations and instabilities of oxidized spiro-OMeTAD concentration in the HTM can dramatically affect device performance, reproducibility, and stability.

Exclusion of oxygen from the atmosphere during device operation could result in a significant advantage in terms of device reliability as it has been well documented that organic molecules readily degrade in the presence of oxygen and light.[14,15] The absorbers in both ssDSSCs and PSCs are also adversely affected by moisture and should be isolated from the humidity present in ambient air to promote device reliability.[16,17]

A number of alternative approaches to improve the conductivity of spiro-OMeTAD have been reported. Cobalt dopants and F4TCNQ have been used to chemically oxidize spiro-OMeTAD.[1,2,18−20] However, peak device performances were achieved while using LiTFSI in the HTM and operating the devices in air. Ionic liquids were recently introduced as effective dopants that do not require the use of LiTFSI but have only been demonstrated effectively in devices operated in air.[21,22]

Methods to directly incorporate an oxidized form of spiro-OMeTAD into the HTM and operate the device in an inert atmosphere have used either 0.24 mol % spiro-OMeTAD^{2+}(PF$_6$)$_2^-$ or 4 mol % spiro-OMeTAD$^+$(CF$_3$SO$_3$)$^-$.[11,23] However, the amounts of oxidized spiro-OMeTAD used in

both studies were significantly lower than the ideal concentration of 10−24 mol %,[11,13] most likely due to solubility limitations. These devices suffered from high series resistance (R_s)[23] and low fill factor (FF) (0.28 vs c. 0.60)[11] as a result. Incorporating a greater amount of oxidized spiro-OMeTAD into the HTM by replacing the PF_6^- or $CF_3SO_3^-$ counteranions with a more soluble group, such as the $(CF_3SO_2)_2N^-$ counteranion employed in this work and used to the same effect in cobalt dopants,[18] can overcome these issues.

The synthesis and use of 2,2′,7,7′-tetrakis(*N*,*N*-di-*p*-methoxyphenylamine)-9,9′-spirobifluorene di[bis-(trifluoromethanesulfonyl)imide], a dicationic salt of spiro-OMeTAD herein abbreviated as spiro(TFSI)$_2$, is presented as an effective means of introducing a highly soluble form of oxidized spiro-OMeTAD to the HTM. Spiro(TFSI)$_2$ is unique in that no chemical additives, such as lithium salts, cobalt complexes, or ionic liquids, are needed to oxidize spiro-OMeTAD in the HTM since spiro(TFSI)$_2$ is in itself simply spiro-OMeTAD that has been "pre-oxidized". Spiro(TFSI)$_2$ can easily be added to the HTM in a desired amount and its high solubility allows for the demonstration of "doping" densities of singly oxidized spiro-OMeTAD in the HTM of up to 28 mol % in a functional device, higher than has been previously reported in the literature.[1,2,11,18−23] With spiro(TFSI)$_2$, the common additive LiTFSI can be removed from the HTM of ssDSSCs and PSCs with no performance loss. The first ssDSSCs fabricated in an oxygen-free environment after dye-sensitization with improved device performance and reproducibility are demonstrated using spiro(TFSI)$_2$.

PSCs fabricated with spiro(TFSI)$_2$ achieve equal power conversion efficiencies (η = 10%) as devices utilizing a conventional spiro-OMeTAD HTM, but showed greater performance stability when constantly illuminated and operated in an inert atmosphere over 10 min, maintaining over 98% peak efficiency versus less than 90% for the standard devices.

■ EXPERIMENTAL SECTION

Complete experimental procedures, synthesis and characterization of spiro(TFSI)$_2$, and device fabrication and testing procedures are provided in the Supporting Information.

■ RESULTS AND DISCUSSION

Synthesis and Characterization. Spiro(TFSI)$_2$ was synthesized by oxidizing spiro-OMeTAD with silver bis-(trifluoromethanesulfonyl)imide (AgTFSI) and was readily isolated in high yield (93%) via precipitation in diethyl ether (Scheme 1; see SI section 1.1 for detailed synthetic procedure). The UV−vis spectra of spiro-OMeTAD, spiro(TFSI)$_2$, and spiro(TFSI) are presented in Figure 1 and closely match previously reported spectra for spiro-OMeTAD, doubly oxidized spiro-OMeTAD, and singly oxidized spiro-OMeTAD.[11,23] The spectrum of singly oxidized spiro-OMeTAD,
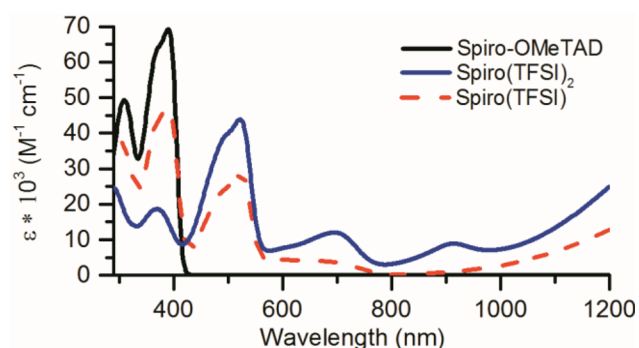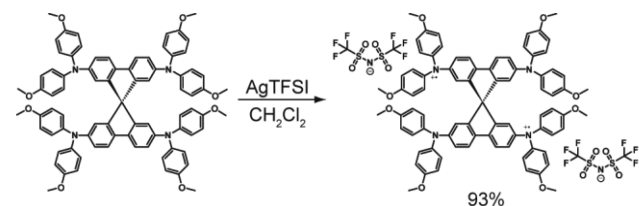
Scheme 1. Synthesis of Spiro(TFSI)$_2$

93%

Figure 1. UV−vis absorption spectra of spiro-OMeTAD, and spiro(TFSI)$_2$, and spiro(TFSI) in chlorobenzene.

in the form of spiro(TFSI), was obtained via titration of a solution of spiro-OMeTAD with exactly 1 equiv of AgTFSI (see SI section 1.10 for detailed procedure).

The ionization potentials (IPs) of spiro-OMeTAD and spiro(TFSI)$_2$, were determined to be −5.05 eV and −5.33 eV, respectively, by photoelectron spectroscopy in air (PESA). These values closely match the difference in oxidation potentials ($\Delta V \sim 0.3$ V) observed with differential pulse voltammetry (DPV) between the neutral and doubly oxidized spiro-OMeTAD species (Table 1). For ease of comparison to

Table 1. Oxidation Potentials of Spiro-OMeTAD as Determined by Differential Pulse Voltammetry[a]

half reaction	$E°$ (eV vs vacuum)
spiro$^0 \rightarrow$ spiro$^+$ + e$^-$	−5.15
spiro$^+ \rightarrow$ spiro^{2+} + e$^-$	−5.27
spiro$^{2+} \rightarrow$ spiro^{3+} + e$^-$	−5.48
spiro$^{3+} \rightarrow$ spiro^{4+} + e$^-$	−6.12

[a]Values based against a ferrocene internal reference taken to be −5.1 eV v vacuum.

the PESA data, the oxidation potentials reported in Table 1 were obtained in reference to a ferrocene internal standard where the redox potential of ferrocene was taken to be −5.1 eV from vacuum, a commonly used method to relate redox potentials obtained electrochemically to the IP of a material (see SI section 1.8 for DVP and cyclic voltammetry spectra).[24]

Energy level band diagrams of TiO$_2$, spiro-OMeTAD, spiro(TFSI)$_2$, and the absorbers WN3.1[25] and CH$_3$NH$_3$PbI$_3$ used in this work's ssDSSCs and PSCs are depicted in Figure 2. The IPs of spiro-OMeTAD, spiro(TFSI)$_2$, WN3.1, and CH$_3$NH$_3$PbI$_3$ were measured using PESA. Although PESA is a surface sensitive technique and cannot probe the effective IP of the various materials at their interfaces, the band offset obtained by comparing PESA results for the CH$_3$NH$_3$PbI$_3$ absorber and spiro-OMeTAD is in good agreement with the reported band offset of the CH$_3$NH$_3$PbI$_3$/spiro-OMeTAD interface using ultraviolet photoemission spectroscopy.[26] The LUMO of WN3.1 and conduction band of CH$_3$NH$_3$PbI$_3$ were calculated as the sum of their respective IPs and optical bandgaps (1.98 eV for WN3.1[25] and 1.56 eV for CH$_3$NH$_3$PbI$_3$[27]). The conduction band energy level of TiO$_2$ was obtained from the literature.[28]

As indicated by the black arrow in Figure 2, substitution of spiro-OMeTAD with spiro(TFSI)$_2$ introduces holes in the valence band of spiro-OMeTAD and shifts the IP of the HTM in a continuum between the IPs of spiro-OMeTAD and
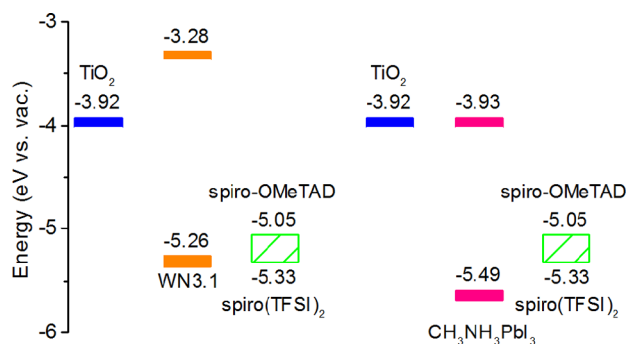
Figure 2. Energy level band diagram of the components of the (a) ssDSSCs and (b) PSCs used in this work. The black arrow indicates a continuous shifting of the bulk HTM ionization potential between the ionization potentials of spiro-OMeTAD and spiro(TFSI)₂ with increasing amounts of spiro(TSFSI)₂.

Figure 3. Normalized UV−vis spectrum of a solution initially containing 86 mol % spiro-OMeTAD and 14 mol % spiro(TFSI)₂ in chlorobenzene (purple solid line). Final solution concentrations of the neutral, singly, and doubly oxidized species were found to be 72.4%, 27.6%, and <0.01%, respectively, by least-squares fit using the individual component spectra of spiro-OMeTAD, spiro(TFSI), and spiro(TFSI)₂ shown in Figure 1.

spiro(TFSI)₂, a process analogous to the use of chemical dopants in polymeric materials that has been well documented in the literature.[8,29] For example, a film containing 14 mol % spiro(TFSI)₂ and 86 mol % spiro-OMeTAD was measured by PESA to have an IP of −5.08 eV, as expected from a linear combination of their individual work functions.

"Doping" Efficiency of Spiro(TFSI)₂. Based on the redox potentials of each oxidation state of spiro-OMeTAD obtained by DPV (Table 1), combining neutral spiro-OMeTAD with spiro(TFSI)₂ will result in a comproportionation reaction between the neutral and doubly oxidized species to form the singly oxidized species at equilibrium. The equilibrium constant of this redox reaction can be calculated using the Nernst equation and redox potentials in Table 1, from which the final concentrations of the neutral, singly, and doubly oxidized species can be derived (see SI section 2 for derivation).

From these basic calculations, a solution initially containing spiro-OMeTAD and 14 mol % spiro(TFSI)₂ should have effectively no spiro(TFSI)₂ remaining at equilibrium with final concentrations of the neutral, singly, and doubly oxidized species of spiro-OMeTAD being 72.3, 27.6, and 0.079 mol %, respectively.

To confirm these expectations, the UV−vis spectrum of a solution containing spiro-OMeTAD and 14 mol % spiro-(TFSI)₂ was fitted with the individual component spectra (Figure 1) of spiro-OMeTAD, spiro(TFSI), and spiro(TFSI)₂, i.e., the neutral, singly, and doubly oxidized species, using nonlinear least-squares curve fitting (Figure 3). The fitted percentages of spiro-OMeTAD, spiro(TFSI), and spiro(TFSI)₂ were 72.4%, 27.6%, and <0.01%, respectively, agreeing well with the predicted equilibrium values. Spiro(TFSI)₂, the doubly oxidized species, was fully consumed to form twice the amount of singly oxidized spiro-OMeTAD in the presence of excess neutral spiro-OMeTAD, effectively demonstrating a near 100% "doping" efficiency. This represents a much higher doping efficiency than the 65−78% reported for cobalt dopants.[2,18]

The UV−vis spectrum of a solution with spiro-OMeTAD and 14 mol % spiro(TFSI)₂ correlated strongly with films deposited from the same solution, with the ratio of oxidized to neutral spiro-OMeTAD observed in solution directly reflecting the ratio in the solid HTM films (see SI section 1.5 for film UV−vis spectrum). The amount of singly oxidized species in the HTM film is thereby easily defined by the amount of spiro(TFSI)₂ added during the preparation of the HTM solution.
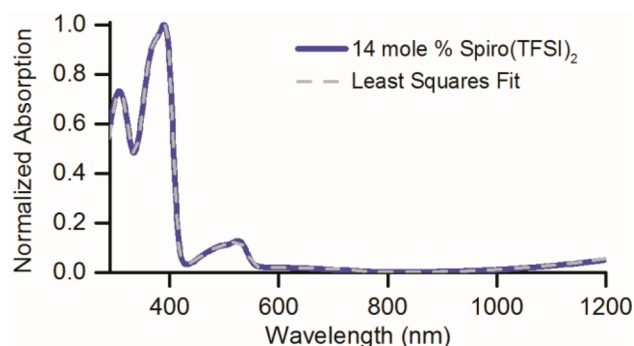
Conductivity Enhancement Using Spiro(TFSI)₂. Four-point probe conductivity measurements of HTM films with between 0 and 16 mol % spiro(TFSI)₂ were acquired (Figure 4;
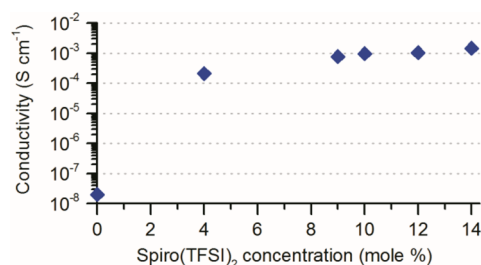

Figure 4. Four-point probe conductivity measurements of HTM films spun on glass from chlorobenzene containing different concentrations of spiro(TFSI)₂. Films were cast and measured at room temperature under a nitrogen atmosphere and dark conditions. All films had the same concentration of the additive tBP and no LiTFSI. Conductivity varies linearly with spiro(TFSI)₂ concentration. Values and a linear fit of the data are available in SI section 1.9.

see SI section 1.9 for film deposition procedures, tabulated conductivity values, and linear fit of data). Deposition and measurement of the films were performed in a nitrogen atmosphere under dark conditions. Films contained the commonly used additive tert-butylpyridine (tBP) but not LiTFSI (conductivity was not affected by the presence of LiTFSI or tBP in an inert atmosphere; see SI section 4). A significant increase in conductivity from 10^{-8} to 10^{-4} S cm^{-1} was observed for even a moderate concentration of 4 mol % spiro(TFSI)₂ with respect to plain spiro-OMeTAD, and a maximum conductivity of 1.43×10^{-3} S cm^{-1} was achieved with a 14 mol % spiro(TFSI)₂ concentration. This is significantly higher than conductivities reported using protic ionic liquids additives with spiro-OMeTAD and comparable to those achieved with cobalt dopants.[2,21] The conductivity of the HTM films varied approximately linearly with spiro(TFSI)₂ concentration, attributable to mainly increasing charge carrier concentration.

Solid-State Dye-Sensitized Solar Cell Performance with Varying Spiro(TFSI)₂ Concentrations. Solid state dye-sensitized solar cells (ssDSSCs) with varying concentrations of spiro(TFSI)₂ in the HTM between 0 and 14 mol %

were fabricated to determine the optimum concentration of spiro(TFSI)$_2$ (see SI section 1.1 for detailed device fabrication procedures). With the exception of the 0 mol % spiro(TFSI)$_2$ (i.e., 100% spiro-OMeTAD) reference point, low concentration values of spiro(TFSI)$_2$ were excluded from this study as has been reported that levels of the singly oxidized species equal to or above 10 mol % (i.e., ≥5 mol % spiro(TFSI)$_2$) are necessary for ideal device performance.[11,13] This high-concentration regime was the focus of this study in order to achieve peak performance in a ssDSSC.

Deposition of titania on conducting glass substrates and dye sensitization with the sensitizer WN3.1[25] were carried out in air. All subsequent fabrication steps, including deposition of the hole-transport layer, contact evaporation, and device testing, were carried out in a controlled, oxygen-free atmosphere. The additive LiTFSI, commonly used to drive the oxidation of spiro-OMeTAD in the presence of oxygen,[11,12] was excluded from the HTM. Its presence was found to have a negligible effect on device performance (see SI section 4 for device metrics of ssDSSCs with and without LiTFSI), demonstrating that the addition of the preoxidized spiro(TFSI)$_2$ fulfilled the same purpose. The additive tBP was used in all devices as its removal significantly decreased all device performance metrics (see SI section 4).

ssDSSC device performance metrics as a function of spiro(TFSI)$_2$ concentration in the HTM, derived from current−voltage measurements in a nitrogen atmosphere, are presented in Figure 5 (see SI section 5 for tabulated values and representative current−voltage curves; R_S was extracted by fitting IV curves to the ideal diode equation). All devices achieved peak performances immediately under a nitrogen atmosphere. In general, increasing the spiro(TFSI)$_2$ concentration decreased the R_S and raised FF monotonically; however, there was a trade-off between FF and J_{SC}/V_{OC}.

Devices with no spiro(TFSI)$_2$ were essentially inoperable, suffering from extremely low J_{SC} and FF and high R_S. The dramatic increase in J_{SC} upon addition of spiro(TFSI)$_2$ can be attributed to improved R_S with increased conductivity of the HTM. Pristine spiro-OMeTAD is essentially a poorly conducting insulator, causing devices to suffer from high R_S due to poor hole-transport through the device. This results in poor charge collection efficiencies as charge recombination dominates over charge transport.[30,31] By improving hole transport through the HTM with the addition of spiro(TFSI)$_2$, a steady reduction of R_S was realized, allowing for improved charge collection efficiency which manifested itself as increased J_{SC}. Similar trends of J_{SC} improvements upon doping of a charge transport layer have been observed in a number of OPV systems, including ssDSSCs using spiro-OMeTAD.[12,31,32] The J_{SC} loss above 9 mol % spiro(TFSI)$_2$ resulted from parasitic absorption of the singly oxidized spiro-OMeTAD species, as its main absorption band (524 nm) overlaps well with that of the sensitizer WN3.1 (534 nm).[25,33]

The steady decrease in V_{OC} with increased spiro(TFSI)$_2$ levels can also be associated with decreased R_S with improved conductivity of the HTM. Although R_S should typically not affect V_{OC}, the higher conductivity of the HTM facilitates charge injection, causing dark current to increase and V_{OC} to decrease (see SI section 5 for dark IV curves). This trend has been observed in other organic photovoltaic devices upon doping.[31]

As FF is greatly affected by R_S,[34] increasing the conductivity of the HTM by increasing the spiro(TFSI)$_2$ concentration
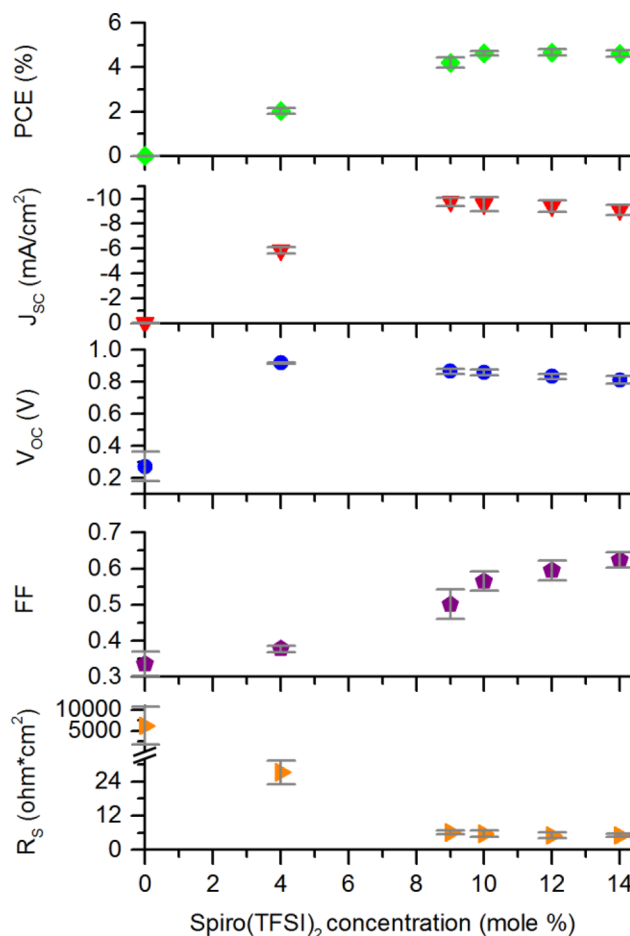

Figure 5. Average device metrics (10 per spiro(TFSI)$_2$ concentration) with standard deviations (gray bars) indicated. Post-dye-sensitization processing and device testing were performed under a nitrogen atmosphere. Devices contained the additive tBP but not LiTFSI.

resulted in a monotonic decrease of series resistance and a corresponding increase in FF. The trade-offs in FF versus J_{SC}/V_{OC} with increase spiro(TFSI)$_2$ concentration resulted in 12 mol % spiro(TFSI)$_2$ to be the optimal amount for peak power conversion efficiency. This corresponds to 24 mol % of the singly oxidized species in the HTM and agrees well with values previously reported in the literature.[13]

Improved Performance and Reproducibility of ssDSSCs without Exposure to Air Using Spiro(TFSI)$_2$. ssDSSCs were fabricated with either a spiro(TFSI)$_2$-based HTM or a conventional spiro-OMeTAD HTM to demonstrate the benefits on device performance and reproducibility that introducing a controlled amount of oxidized spiro-OMeTAD to the HTM with spiro(TFSI)$_2$ has rather than relying on the conventional method of oxidizing spiro-OMeTAD in air with LiTFSI. Devices were sensitized with the WN3.1 dye. Post-sensitization, all devices were fabricated and initially tested in a nitrogen atmosphere. The spiro(TFSI)$_2$-based HTM contained the optimal 12 mol % spiro(TFSI)$_2$ concentration along with the additive tBP. The conventional spiro-OMeTAD HTM contained pristine spiro-OMeTAD, LiTFSI, and tBP.

Devices using the conventional HTM and never exposed to air were not operable. Peak power conversion efficiencies were only achieved after 9−16 h of exposure to air and light, a commonly used "light-soaking" practice necessary to generate oxidized spiro-OMeTAD in the HTM with LiTFSI.[11,12] These

conventional devices also suffered from significant variations in performance (Figure 6), attributed to the uncontrollability of generating oxidized spiro-OMeTAD with LiTFSI in air.

Figure 6. Histogram of ssDSSCs containing either an optimized 12 mol % spiro(TFSI)$_2$/tBP HTM or a conventional spiro-OMeTAD/tBP/LiTFSI HTM. All devices were fabricated in a nitrogen atmosphere post-sensitization. Reported efficiencies for conventional devices were obtained in air while those of spiro(TFSI)$_2$-based devices were obtained in a nitrogen atmosphere. Fifteen devices per HTM formulation (0.1% bin size).

In contrast, devices using the optimized spiro(TFSI)$_2$ HTM had better average V_{OC}, J_{SC}, FF, and power conversion efficiency along with a much tighter spread in performance compared to the conventional devices (Figure 6; see SI section 6 for average device metrics and representative IV curves). Noteworthy was that the spiro(TFSI)$_2$-based devices immediately achieved their highest performance in a nitrogen atmosphere with no required light-soaking. By introducing oxidized spiro-OMeTAD in a controlled manner using spiro(TFSI)$_2$ instead of the conventional LiTFSI-based approach, ssDSSCs can attain higher and more reproducible device performances when prepared and operated under an oxygen-free atmosphere.

Spiro(TFSI)$_2$ in Nanostructured Perovskite Solar Cells. Highly efficient perovskite-absorber solar cells (PSCs) and ssDSSCs both utilize spiro-OMeTAD as the HTM.[1,2,35] However, these reported devices were operated in ambient air to achieve their peak efficiencies. To improve device stability, exposure of devices to ambient air and moisture should be minimized to avoid degradation of the absorber and organic HTM from moisture and photo-oxidation. Spiro-(TFSI)$_2$ can be used to increase the conductivity of the spiro-OMeTAD HTM in PSCs without the need to maintain an oxygen presence for optimal device performance. PSCs using a $CH_3NH_3PbI_3$ absorber on mesoporous TiO_2 were fabricated in a nitrogen atmosphere with either the optimized spiro(TFSI)$_2$ HTM or a conventional spiro-OMeTAD HTM described in the previous section (see SI section 1.3 for device fabrication details). Both HTM solutions were processed under the same conditions, resulting in HTMs that were 100 ± 30 nm thick in all devices (see SI section 7 for representative cross-sectional SEM). Devices were tested using a 5 s delay time at each voltage step prior to measuring current. Under such conditions, stable device performance was observed, with no hysteretic behavior between forward or reverse scan directions (see SI section 7 for representative IV curves).

Devices containing the spiro(TFSI)$_2$ HTM were moderately functional (η = 6%) when never exposed to air, while those with the conventional HTM did not function at all (Figure 7).
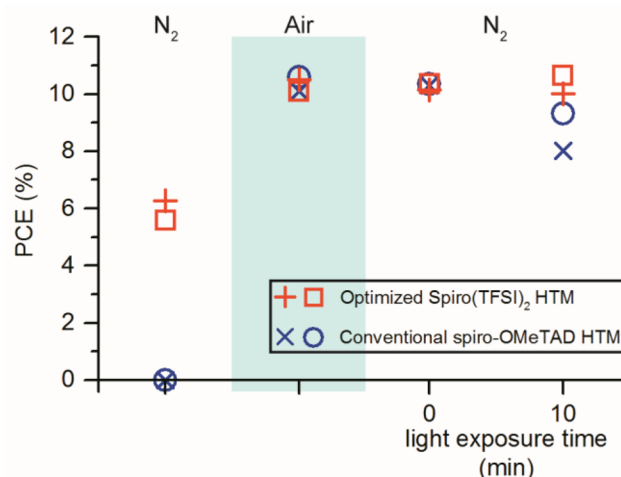

Figure 7. Power conversion efficiencies of PSCs with either a 12 mol % spiro(TFSI)$_2$ HTM or conventional spiro-OMeTAD HTM under three consecutive environmental testing conditions: (1) nitrogen atmosphere, never exposed to air; (2) exposed to air; (3) reintroduced to a nitrogen atmosphere after being exposed to air. Upon reintroduction to a nitrogen atmosphere, devices with spiro(TFSI)$_2$ maintained greater than 98% of initial efficiencies after 10 min of illumination compared to less than 90% for devices without.

However, unlike the ssDSSCs in this study that used spiro(TFSI)$_2$ and achieved their highest efficiencies when never exposed to air, all PSCs required exposure to air to improved their peak efficiencies up to η = 10% (see SI section 4 for effects of exposing ssDSSCs to air; see SI section 7 for PSC device current–voltage metrics). While the role of oxygen has not been well characterized in PSCs, it is hypothesized that oxygen aids in surface passivation of the perovskite absorber.

After exposure to air, the devices were reintroduced and operated under a nitrogen atmosphere to simulate encapsulation of the devices in an oxygen- and moisture-free environment. All devices initially performed at their peak, air-exposed efficiencies (Figure 7). However, only devices with spiro-(TFSI)$_2$ were able to maintain a stable performance (greater than 98% of initial performance) over 10 min of constant illumination and operation at AM1.5, while those with the conventional HTM maintained no more than 90% of their initial performance.

The rapid decrease in performance of the devices without spiro(TFSI)$_2$ could be a result of the reversible oxidation reaction of a conventional spiro-OMeTAD HTM.[13] While LiTFSI is used to drive the oxidation of spiro-OMeTAD forward in the presence of oxygen, removal of oxygen could shift the equilibrium back toward the reductive reaction where the Li$^+$ end product, possibly a lithium oxide,[11,12] and oxidized spiro-OMeTAD are consumed to reform neutral spiro-OMeTAD. This would lead to a lower charge carrier concentration and conductivity of the HTM, diminishing device performance over time as oxidized spiro-OMeTAD is consumed. Devices utilizing spiro(TFSI)$_2$ circumvented this issue by directly introducing a stable amount of oxidized spiro-OMeTAD to the HTM to improve its conductivity without the use of LiTFSI. With no lithium species present in the HTM to

promote the formation or depletion of oxidized spiro-OMeTAD, these devices were able to maintain stable performance over a 10 min period of constant illumination and operation in an oxygen-free atmosphere. Such operating stability will be highly beneficial to the commercialization of PSCs as they will require encapsulation in an inert, moisture-free environment to promote long-term stability.

CONCLUSION

Spiro($TSFI)_2$, a dicationic salt of spiro-OMeTAD, provides an efficient means of controllably increasing the conductivity of the spiro-OMeTAD HTM commonly used in ssDSSCs and PSCs by introducing the singly oxidized spiro-OMeTAD species with near 100% efficiency. Controlling the amount of oxidized spiro-OMeTAD in the HTM with spiro($TFSI)_2$ resulted in higher and more reproducible ssDSSC device performance and improved operating stability of efficient PSCs in an inert atmosphere. Using spiro($TFSI)_2$ will help to facilitate the commercialization of these technologies by enabling sealing in a dry, oxygen-free environment to avoid potential degradation of the absorbers and organic materials by moisture and photo-oxidation.

ASSOCIATED CONTENT

ⓈSupporting Information

Additional figures, data, and detailed synthetic preparation and characterization procedures of spiro($TFSI)_2$. This material is available free of charge via the Internet at http://pubs.acs.org.

AUTHOR INFORMATION

Corresponding Author
*E-mail: mmcgehee@stanford.edu.

Notes
The authors declare no competing financial interest.

ACKNOWLEDGMENTS

REFERENCES

(1) Burschka, J.; Pellet, N.; Moon, S.-J.; Humphry-Baker, R.; Gao, P.; Nazeeruddin, M. K.; Grätzel, M. *Nature* **2013**, *499*, 316.

(2) Burschka, J.; Dualeh, A.; Kessler, F.; Baranoff, E.; Cevey-Ha, N.-L.; Yi, C.; Nazeeruddin, M. K.; Grätzel, M. *J. Am. Chem. Soc.* **2011**, *133*, 18042.

(3) Best Research-Cell Efficiencies, rev 04−24−2014 http://www.nrel.gov/ncpv/images/efficiency_chart.jpg.

(4) Hagfeldt, A.; Boschloo, G.; Sun, L.; Kloo, L.; Pettersson, H. *Chem. Rev.* **2010**, *110*, 6595.

(5) Ball, J. M.; Lee, M. M.; Hey, A.; Snaith, H. J. *Energy Environ. Sci.* **2013**, *6*, 1739.

(6) Heo, J. H.; Im, S. H.; Noh, J. H.; Mandal, T. N.; Lim, C.-S.; Chang, J. A.; Lee, Y. H.; Kim, H.; Sarkar, A.; Nazeeruddin, M. K.; Grätzel, M.; Seok, S. Il. *Nat. Photonics* **2013**, *7*, 486.

(7) Leijtens, T.; Lim, J.; Teuscher, J.; Park, T.; Snaith, H. J. *Adv. Mater.* **2013**, *25*, 3227.

(8) MacDiarmid, A. G. *Angew. Chem., Int. Ed.* **2001**, *40*, 2581.

(9) Bach, U.; Lupo, D.; Comte, P.; Moser, J.; Weissörtel, F.; Salbeck, J.; Spreitzer, H.; Grätzel, M. *Nature* **1998**, *395*, 583.

(10) Snaith, H. J.; Grätzel, M. *Appl. Phys. Lett.* **2006**, *89*, 262114.

(11) Cappel, U. B.; Daeneke, T.; Bach, U. *Nano Lett.* **2012**, *12*, 4925.

(12) Abate, A.; Leijtens, T.; Pathak, S.; Teuscher, J.; Avolio, R.; Errico, M. E.; Kirkpatrik, J.; Ball, J. M.; Docampo, P.; McPherson, I.; Snaith, H. J. *Phys. Chem. Chem. Phys.* **2013**, *15*, 2572.

(13) Schölin, R.; Karlsson, M. H.; Eriksson, S. K.; Siegbahn, H.; Johansson, E. M. J.; Rensmo, H. *J. Phys. Chem. C* **2012**, *116*, 26300.

(14) Tidwell, T. *Nat. Chem.* **2013**, *5*, 637.

(15) Neugebauer, H.; Brabec, C. J.; Hummelen, J. C.; Janssen, R. a. J.; Sariciftci, N. S. *Synth. Met.* **1999**, *102*, 1002.

(16) Tennakone, K.; Kumara, G. R. R. A.; Kottegoda, I. R. M.; Wijayantha, K. G. U. *Semicond. Sci. Technol.* **1997**, *12*, 128.

(17) Noh, J. H.; Im, S. H.; Heo, J. H.; Mandal, T. N.; Seok, S. Il. *Nano Lett.* **2013**, *13*, 1764.

(18) Burschka, J.; Kessler, F.; Nazeeruddin, M. K.; Grätzel, M. *Chem. Mater.* **2013**, *25*, 2986.

(19) Chen, D.-Y.; Tseng, W.-H.; Liang, S.-P.; Wu, C.-I.; Hsu, C.-W.; Chi, Y.; Hung, W.-Y.; Chou, P.-T. *Phys. Chem. Chem. Phys.* **2012**, *14*, 11689.

(20) Noh, J. H.; Jeon, N. J.; Choi, Y. C.; Nazeeruddin, M. K.; Grätzel, M.; Seok, S. Il. *J. Mater. Chem. A* **2013**, *1*, 11842.

(21) Abate, A.; Hollman, D. J.; Teuscher, J.; Pathak, S.; Avolio, R.; D'Errico, G.; Vitiello, G.; Fantacci, S.; Snaith, H. J. *J. Am. Chem. Soc.* **2013**, *135*, 13538.

(22) Zhang, H.; Shi, Y.; Yan, F.; Wang, L.; Wang, K.; Xing, Y.; Dong, Q.; Ma, T. *Chem. Commun. (Camb.)* **2014**, *50*, 5020.

(23) Bach, U. Ph.D. Thesis. Ecole polytechnique fédérale de Lausanne; Lausanne, Switzerland, 2000.

(24) Cardona, C. M.; Li, W.; Kaifer, A. E.; Stockdale, D.; Bazan, G. C. *Adv. Mater.* **2011**, *23*, 2367.

(25) Nguyen, W. H.; Bailie, C. D.; Burschka, J.; Moehl, T.; Grätzel, M.; McGehee, M. D.; Sellinger, A. *Chem. Mater.* **2013**, *25*, 1519−1525.

(26) Schulz, P.; Edri, E.; Kirmayer, S.; Hodes, G.; Cahen, D.; Kahn, A. *Energy Environ. Sci.* **2014**, *7*, 1377.

(27) Kulkarni, S. A.; Baikie, T.; Boix, P. P.; Yantara, N.; Mathews, N.; Mhaisalkar, S. *J. Mater. Chem. A* **2014**, *2*, 9221.

(28) Grancini, G.; Santosh Kumar, R. S.; Abrusci, A.; Yip, H.-L.; Li, C.-Z.; Jen, A.-K. Y.; Lanzani, G.; Snaith, H. J. *Adv. Funct. Mater.* **2012**, *22*, 2160.

(29) Zhang, Y.; Zhou, H.; Seifter, J.; Ying, L.; Mikhailovsky, A.; Heeger, A. J.; Bazan, G. C.; Nguyen, T.-Q. *Adv. Mater. (Deerfield Beach, Fla.)* **2013**, *25*, 7038−7044.

(30) Marsh, R. a.; Groves, C.; Greenham, N. C. *J. Appl. Phys.* **2007**, *101*, 083509.

(31) Umeda, T. *J. Photonics Energy* **2011**, *1*, 011113.

(32) Nakayama, K.; Matsui, Y.; Yokoyama, M. *Jpn. J. Appl. Phys.* **2005**, *44*, 633.

(33) Margulis, G. Y.; Hardin, B. E.; Ding, I.; Hoke, E. T.; McGehee, M. D. *Adv. Energy Mater.* **2013**, *3*, 959.

(34) Wolf, M.; Rauschenbach, H. *Adv. Energy Convers.* **1963**, *3*, 455.

(35) Liu, M.; Johnston, M. B.; Snaith, H. J. *Nature* **2013**, *501*, 395.